https://doi.org/10.35877/jetech4580

OPEN ACCESS

ISSN : 2776-7914 (Print) / 2807-3045 (Online)

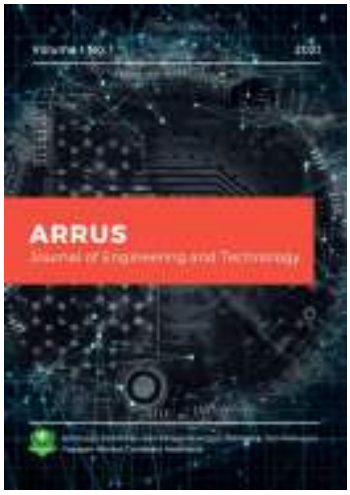

RESEARCH ARTICLE

Improving the Accuracy of Ground Displacement Estimation Using IMU with Low-Pass Butterworth Filter

Kartiko Ardi Widodo[1], and Bima Romadhon Parada Dian Palevi[2], Nanta Sigit[3]

[1,2] Electrical Engineering Department, National Institute of Technology Malang, Malang, Indonesia
[3] Industrial Engineering, Universitas Wisnuwardhana, Malang, Indonesia

*Corresponding author: Kartiko Ardi Widodo, Electrical Engineering Department, National Institute of Technology Malang, Malang, Indonesia

E-mail: tiko_ta@lecturer.itn.ac.id

Abstract: Land deformation monitoring typically relies on GNSS and InSAR, which face limitations in costs and signal accessibility. As a portable alternative, the Inertial Measurement Unit (IMU), which utilizes an internal Accelerometer to record data, offers a flexible solution for environments where external signals are obstructed. However, the primary challenge in using an IMU for precise Measurement is the presence of high-frequency Noise and integration errors, which lead to significant drift in Displacement estimates. This research proposes integrating the Zero-Velocity Update (ZUPT) method with a second-order Butterworth low-pass filter to address these inaccuracies. Testing results for Displacement values between 10–30 cm showed a dramatic improvement in reliability. Without the filter, the estimation yielded an RMSE of 0.4292 m and a Relative Error of Prediction (REP) of –304.8%. After applying the Butterworth filter to mitigate sensor Noise, the RMSE dropped to 0.002 m with an REP of only –0.40%, representing an error reduction of over 99%. These findings confirm that the refined IMU system is a highly accurate tool for real-time land deformation monitoring, providing a robust alternative to traditional methods in challenging terrains.

Keywords: Accellerometer, Displacement, IMU, Measurement, Noise.

1. INTRODUCTION

Landslides are one of the most frequent geological disasters in Indonesia, with significant impacts on people, infrastructure, and the environment. Geographical factors, such as high rainfall, steep topography, land-use changes, and human activity, increase the vulnerability and frequency of landslides (Ruzza et al., 2020)]. One of the early indicators of a landslide is ground shifting, so deformation monitoring technology plays an important role in disaster mitigation. (Ahmad Sheikh et al., 2025).

Ground movement monitoring is also carried out using geotechnical sensors such as inclinometers (F. Yang et al., 2025), tilt meters (Z. Zhang et al., 2021), and extensometers (Elhag et al., 2025). Inclinometers measure changes in slope angle, tilt meters detect small rotations in the soil structure, and extensometers are used to monitor changes in the distance between cracks or fissures. While effective in early deformation detection, geotechnical sensors have limitations such as a limited number of measurement points, high installation costs, and complex maintenance, especially on a large scale or in remote areas. Their application in caves also poses technical challenges, such as difficulty installing on uneven surfaces and limited access for routine maintenance.

https://doi.org/10.35877/jetech4580

ISSN : 2776-7914 (Print) / 2807-3045 (Online)

Global Navigation Satellite System (GNSS) based technology (Piter et al., 2024) and Interferometric Synthetic Aperture Radar (InSAR) (Bao et al., 2025) GNSS has been widely used due to its high accuracy and ability to detect deformation at various scales. GNSS, particularly differential methods, can provide positioning accuracy down to the centimeter or even millimeter level. However, GNSS has limitations, including high equipment costs and the need for communication infrastructure for real-time data transmission (Goanta, 2020).

Furthermore, various studies have proposed methods to improve GNSS accuracy and robustness, such as utilizing GNSS reflected signals with Track-before-Detect (TbD) (Haji-Aghajany et al., 2025). Wang at 2021, integrating multiple GNSS with Precise Point Positioning (PPP) and PPP-RTK techniques (Yong et al., 2022), and measuring seafloor deformation using GNSS-Acoustic (Yong et al., 2022). However, the main challenges with GNSS remain related to signal limitations in confined areas, infrastructure costs, and the need for complex data correction.

On the other hand, InSAR offers the ability to detect surface deformation over large areas at millimeter resolution (MacAfee et al., 2024). This method has proven effective in monitoring landslides, subsidence, and deformation caused by volcanic activity. However, InSAR's limitations lie in its relatively long image acquisition interval, sensitivity to atmospheric conditions, vegetation, and soil moisture, and limited applicability to small objects.

These fundamental limitations of GNSS and InSAR indicate a gap in land deformation monitoring, particularly in locations difficult to reach by satellites and applications requiring real-time data. To bridge this gap, alternative technologies are needed that are accurate, low-cost, flexible, and capable of operating under extreme conditions (Parlin et al., 2024).

In this context, the Inertial Measurement Unit (IMU) offers a potential solution. IMUs work without relying on external signals, are small, relatively inexpensive, and flexible for installation in a variety of applications and location. Various approaches have been developed to optimize IMU performance, including dead reckoning methods, the Kalman Filter and its variants (EKF, UKF), Zero Velocity Update (ZUPT), and integration with GNSS or IoT. However, the main challenges of IMUs are long-term drift accumulation and sensitivity to sensor noise (Tjahjono et al., 2024).

Based on these studies, this research contributes to the development of an IMU-based method optimized for monitoring ground displacement in enclosed areas, such as caves or tunnels, where GNSS and InSAR are ineffective. The novelty of this research lies in the application of a Butterworth Low-Pass Filter to improve the accuracy of ground displacement estimation using IMU. Thus, IMU is positioned not as a replacement for GNSS or InSAR, but as a complementary technology that extends monitoring coverage to extreme locations that are difficult to reach by satellite-based technology (Z. Yang et al., 2025).

Although IMUs offer the advantages of small size, low cost, and installation flexibility, the main challenges they face are drift and noise due to the integration of acceleration into displacement calculations. This accumulated error can increase over time if not corrected. To address this, various filtering methods such as the Kalman Filter, Complementary Filter, and machine learning-based approaches have been developed. However, most research still focuses on surface infrastructure such as bridges and buildings, while specific applications for monitoring landslide potential in enclosed areas, such as caves, are still very limited. This indicates a significant research gap: the need to optimize IMUs as a low-cost, adaptive, real-time monitoring solution that can be implemented in locations beyond the reach of GNSS or remote sensing technology (X. Zhang et al., 2025)

This paper is structured as follows. The first section presents an introduction covering the background, problem, previous studies, contributions, and structure of the paper. The second section describes the research methodology, including the system design and algorithms used. The third section presents the experimental results and analysis. The fourth section discusses

https://doi.org/10.35877/jetech4580

ISSN : 2776-7914 (Print) / 2807-3045 (Online)

the main findings, strengths, and limitations of the proposed approach. The final section concludes the research and provides directions for further development (Sheikh et al., 2021).

2. Literature Review

2.1. *Type and Research Approach*

This study is an experimental research with a quantitative approach. The objective is to evaluate the accuracy of ground displacement estimation using an Inertial Measurement Unit (IMU) with the application of a low-pass Butterworth filter (Sari et al., 2024).

2.2. *Research Object and Location*

The research object is an IMU module with a three-axis accelerometer sensor, focused on the X and Y axes (the Z axis is disregarded). The experiment was conducted in a laboratory using a flat table with a length of 50 cm as the medium, with actual displacement variations of 10 cm, 20 cm, 30 cm, 40 cm, and 50 cm (Figure 2).

2.3. *Research Instruments*

The instruments used in this study include:

Main sensor: IMU with a three-axis accelerometer.

Acquisition unit: microcontroller for recording acceleration data at a 100 Hz sampling frequency.

Signal filter: second-order low-pass Butterworth filter with a cutoff frequency of 5 Hz.

Reference measurement tool: mechanical ruler with 1 mm resolution as the ground truth.

2.4. *Experimental Design*

The experiment was conducted by placing the sensor on a box that was moved translationally on a 50 cm flat table. The actual displacements were varied between 10–50 cm and measured using the mechanical ruler. To maintain consistency, the movements were performed at a relatively constant speed to minimize extreme acceleration variations. Each test scenario was repeated five times (Cahyadi et al., 2024).

2.5. *Research Stages*

The research stages consist of:

Data acquisition: recording acceleration data at a 100 Hz sampling frequency.

Data preprocessing: bias correction by calculating the mean acceleration in a static condition, followed by signal filtering using a second-order Butterworth filter.

Displacement estimation: double integration of the acceleration signal, with the application of the Zero-Velocity Update (ZUPT) method to reduce error drift.

Result evaluation: comparing the estimated displacement with the ground truth.

2.6. *Research Variables*

Independent variables: actual displacement values (10–50 cm) and filter condition (with/without filter).

Dependent variable: IMU-based displacement estimation results.

Control variables: sampling frequency (100 Hz), table path, and relatively constant movement speed.

3. Research Method

3.1. *Data Analysis Method*

https://doi.org/10.35877/jetech4580

ISSN : 2776-7914 (Print) / 2807-3045 (Online)

Quantitative analysis was carried out using two main indicators: Root Mean Square Error (RMSE) to measure the deviation of the estimation from the actual value, and Relative Error Percentage (REP) to assess the level of relative error in each displacement scenario. The analysis was performed comparatively by evaluating system performance under both unfiltered and filtered conditions (Van Natijne et al., 2022).

3.2. *Data Acquisition*

The primary sensor used in this study is a three-axis accelerometer (the z-axis is ignored) with a sampling frequency of 100 Hz. Experiments were conducted on a flat table surface, with actual displacement measured using a millimeter-resolution mechanical ruler as ground truth. Acceleration data was recorded via a microcontroller and stored on a computer for further processing.

3.3. *Data Preprocessing*

The raw signal generated by an accelerometer generally contains noise, bias, and drift, so a preprocessing stage is required before displacement estimation can be performed. The first step is bias correction, which calculates the initial offset under static conditions as the average acceleration value, then subtracts it from the measured signal. This correction process is expressed in Eq. (1):

$$a_i' = a_i - \bar{a}_{static} \quad (1)$$

where a_i is the corrected acceleration and $\bar{a}_{static}$ is the average value of the acceleration under static conditions.

The second stage is signal filtering using a second-order Butterworth low-pass filter with a cutoff frequency of 5 Hz. The primary purpose of this filtering is to reduce high-frequency noise from environmental vibrations and electronic interference. The Butterworth filter was chosen because of its flat response across the passband, thus minimizing distortion in the primary signal.

3.4. *Displacement Estimation*

Next, displacement estimation is performed by double integration of the acceleration signal. In the first stage, the velocity is calculated by integrating over the acceleration, as shown in Eq. (2):

$$v(t) = \int a(t)dt \quad (2)$$

and displacement is calculated by second integration, in Eq. 3.

$$s(t) = \int v(t)dt = \iint a(t)dt^2 \quad (3)$$

However, the dual integration of acceleration is highly susceptible to error drift. To address this, the Zero-Velocity Update (ZUPT) method is used, which assumes zero velocity when the sensor is in a static state (Eq. (4)).

$$v(tk) = 0 \, (4)$$

Static conditions are determined when the standard deviation of acceleration is less than a certain threshold (e.g. < 0.02 g).

3.5. *Evaluation of Results*

Evaluation of the results was performed by comparing the displacement estimates to the ground truth obtained using a millimeter-resolution mechanical ruler. Two main metrics were used: Root Mean Square Error (RMSE) (Eq. (5)),

$$RMSE = \sqrt{\frac{1}{n}\sum_{i=1}^{n}\left(d_i - \hat{d}_i\right)^2} \quad (5)$$

https://doi.org/10.35877/jetech4580

ISSN : 2776-7914 (Print) / 2807-3045 (Online)

and Relative Error Percentage (REP) (Eq. (6))

$$REP = \frac{|d-\hat{d}|}{d}.100\% \qquad (6)$$

With d_i actual displacement and $\hat{d}_i$ displacement estimation results.

Table 1. Effect of Filter Bandwidth on Accelerometer Noise and SNR

BW (Hz)	Noise (g)			Signal + Noise			SNR Linear			SNR (dB)		
	X	Y	Z	X	Y	Z	X	Y	Z	X	Y	Z
-	0.033	0.040	0.186	0.316	0.329	0.335	9.515	8.199	1.798	19.56	18.27	5.095
460	0.020	0.024	0.075	0.316	0.320	0.324	15.96	13.43	4.324	24.06	22.56	12.71
184	0.018	0.021	0.095	0.318	0.316	0.325	17.49	15.35	3.406	24.85	23.72	10.64
92	0.019	0.018	0.087	0.323	0.321	0.325	16.89	17.45	3.715	24.55	24.83	11.40
41	0.009	0.015	0.092	0.318	0.317	0.324	35.74	20.86	3.540	31.06	26.38	10.97
20	0.010	0.008	0.093	0.317	0.316	0.323	33.35	42.08	3.476	30.46	32.48	10.82
10	0.004	0.005	0.089	0.320	0.320	0.325	76.09	66.73	3.661	37.62	36.48	11.27
5	0.002	0.005	0.085	0.317	0.319	0.323	198.2	67.79	3.805	45.94	36.62	11.60

Table 2. Displacement Estimation Results Using IMU (Without Filter)

No.	Actual Disp (m)	IMU Estimation (m)					
		Trial 1	Trial 2	Trial 3	Trial 4	Trial 5	Average
1	0.10	0.365	0.386	0.395	0.437	0.593	0.4352
2	0.20	0.385	0.392	0.421	0.503	1.445	0.6292
3	0.30	0.359	0.365	0.367	0.382	0.456	0.3858
4	0.40	0.556	0.556	0.556	0.556	0.556	0.556
5	0.50	0.768	0.793	0.869	0.872	0.882	0.8368

4. Results and Discussion

4.1. Calibration Results and Noise Reduction

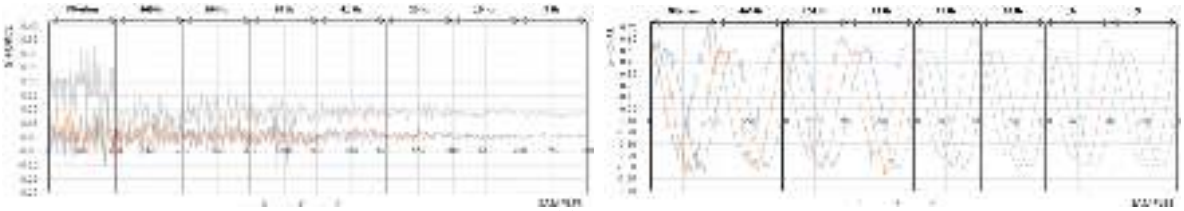

Fig. 1. Noise reduction visualization (Left Side). The effect of bandwidth on noise-reduced signals (Right Side).

Table 1 shows the results of noise measurements, total signal (signal + noise), and signal-to-noise ratio (SNR) in linear and decibel (dB) forms on the X, Y, and Z axes with varying bandwidth (BW). In conditions without a bandwidth filter, the noise value is relatively high, namely 0.033 g (X), 0.040 g (Y), and 0.186 g (Z), resulting in a low SNR, especially on the Z axis (5.095 dB). However, after the bandwidth is narrowed, there is a significant decrease in the noise value.

https://doi.org/10.35877/jetech4580

ISSN : 2776-7914 (Print) / 2807-3045 (Online)

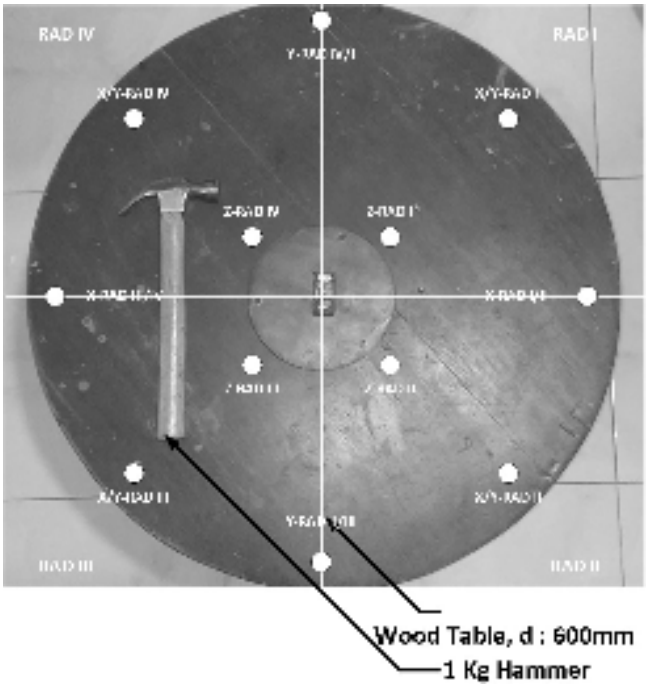

Fig. 2. Sensors On The Test Bench.

For example, at a BW of 5 Hz, the noise decreases to 0.002 g (X), 0.005 g (Y), and 0.085 g (Z). Consequently, the SNR increases sharply especially on

Table 3. Displacement Estimation Results Using IMU (With Filter)

No.	Actual Disp (m)	IMU Estimation (m)					
		Trial 1	Trial 2	Trial 3	Trial 4	Trial 5	Average
1	0.10	0.113	0.122	0.123	0.154	0.164	0.1352
2	0.20	0.195	0.204	0.211	0.216	0.221	0.2094
3	0.30	0.316	0.319	0.338	0.348	0.351	0.3344
4	0.40	0.409	0.409	0.409	0.409	0.409	0.409
5	0.50	0.49	0.497	0.501	0.51	0.512	0.502

Table 4. RMSE and REP Analysis (Without Filter)

No.	Actual Disp (m)	Avg IMU Est (m)	RMSE	REP (%)
1	0.10	0.4352	0.3352	-335.20%
2	0.20	0.6292	0.4292	-214.60%
3	0.30	0.3858	0.0858	-28.60%
4	0.40	0.556	0.156	-39.00%
5	0.50	0.8368	0.3368	-67.36%

the X and Y axes. At a BW of 5 Hz, the SNR reaches 198.2 (45.94 dB) on the X axis and 67.79 (36.62 dB) on the Y axis. In contrast, the Z axis still shows relatively low SNR values, ranging from 1.798 to 3.805 (5.095–11.60 dB), although there is also a slight improvement when the bandwidth is smaller. The visualization of noise reduction is shown in Figure 1 top side, while the effect of bandwidth on the noise-reduced signal is shown in Figure 1 bottom side.

4.2. Displacement Estimation Results Before Filtering

The initial stage of displacement estimation is performed after bias correction, but without filtering the acceleration signal. The raw data still contains high-frequency noise

https://doi.org/10.35877/jetech4580

ISSN : 2776-7914 (Print) / 2807-3045 (Online)

(approximately <0.02 g) originating from environmental vibrations, sensor imperfections, and electronic interference. When these signals are double-integrated to obtain displacement, the accumulated noise results in significant errors. Table 2 presents the results of displacement estimation using the IMU without filtering. In the first trial with an actual displacement of 0.10 m, the IMU estimate showed an average value of 0.4352 m, significantly higher than the actual value. In the second trial with an actual displacement of 0.20 m, the estimate deviated further, with an average of 0.6292 m, even reaching 1.445 m in the fifth trial. Conversely, in the third trial with an actual displacement of 0.30 m, the average estimate was closer to the actual condition, at 0.3858 m. Meanwhile, at a displacement of 0.40 m, the estimate was consistent across all trials at 0.556 m. For the fifth experiment with an actual displacement of 0.50 m, the IMU estimate averaged 0.8368 m, again indicating an overestimation of the actual value. Overall, this table indicates that displacement estimates using an unfiltered IMU tend to deviate significantly from the actual value, with a dominant pattern of overestimation, especially for small displacements (0.10–0.20 m) and larger displacements (0.50 m).

4.3. Displacement Estimation Results After Filtering

To improve accuracy, the acceleration signal was then processed using a second-order Butterworth low-pass filter with a cutoff frequency of 5 Hz. This filter was chosen because of its stable characteristics and flat response across the passband, effectively suppressing high-frequency noise components without distorting the main signal components associated with slow translational motion. Table 3 shows the displacement estimation results using the IMU after applying the filter. In contrast to the unfiltered condition, the displacement estimates appear much closer to the actual values. At an actual displacement of 0.10 m, the IMU estimates averaged 0.1352 m, only slightly larger than the actual value. At a displacement of 0.20 m, the average estimate was 0.2094 m, with relatively small inter-trial variation (0.195–0.221 m). Similarly, at a displacement of 0.30 m, the average estimate was 0.3344 m, still within a range close to the actual condition. Furthermore, at a displacement of 0.40 m, the estimation results were very consistent, with all trials showing the same value of 0.409 m. For a displacement of 0.50 m, the average estimated value is 0.502 m, indicating very high accuracy with minimal deviation.

4.4. Quantitative Evaluation with RMSE and REP

Table 4 presents the results of error analysis using Root Mean Square Error (RMSE) and Relative Error

Table 5. RMSE and REP Analysis (With Filter)

No.	Actual Disp (m)	Avg IMU Est (m)	RMSE	REP (%)
1	0.10	0.1352	0.0352	-35.20%
2	0.20	0.2094	0.0094	-4.70%
3	0.30	0.3344	0.0344	-11.47%
4	0.40	0.409	0.009	-2.25%
5	0.50	0.502	0.002	-0.40%

Percentage (REP) on the IMU displacement estimation without a filter. The results show a significant deviation between the actual and estimated displacement. At a displacement of 0.10 m, the RMSE value reaches 0.3352 with an REP of –335.20%, indicating a significant overestimation. A similar condition occurs at a displacement of 0.20 m with an RMSE of 0.4292 and an REP of –214.60%. Even at a larger displacement (0.50 m), the RMSE value is still high (0.3368) with an REP of –67.36%. Overall, without a filter, the IMU tends to produce large and inconsistent errors, especially at small displacements.

In contrast, Table 5 shows the results of the RMSE and REP analysis after applying the filter. The estimation performance improves significantly with a much smaller error. At a

https://doi.org/10.35877/jetech4580

ISSN : 2776-7914 (Print) / 2807-3045 (Online)

displacement of 0.10 m, the RMSE is only 0.0352 with an REP of –35.20%, indicating a significant improvement in accuracy compared to the unfiltered condition. At displacements of 0.20 m and 0.30 m, the REP values drop drastically to –4.70% and –11.47%, respectively. The displacement estimates of 0.40 m and 0.50 m even have very small deviations, with REPs of only –2.25% and –0.40%.

4.5. Advantages of the IMU Approach

The test results are shown in Figure 3 and Figure 4. At this stage, the ZUPT method was replicated without the addition of a digital filter as described in previous research in the Methods Chapter. Next, the results were compared with the application of the ZUPT method integrated with a Low-Pass Butterworth Filter. The results of the replication of the previous research are presented in Figure 4, while the results with the addition of a filter are presented in Figure 3.

Figure 3 presents five graphs of displacement testing over a distance of 10 cm along the X-axis, each conducted five times, with additional evaluation of deviations along the Z-axis and quantitative assessment using RMSE and REP.

The first graph (topmost) shows measurement results of 0.113 m, 0.122 m, 0.123 m, 0.154 m, and 0.164 m. The average value obtained was 0.1352 m, indicating a considerable positive deviation compared to the actual displacement of 0.10 m. Deviations along the Z-axis ranged from 0.422 m to 1.4 m, suggesting significant noise in the non-motion direction. Quantitative evaluation yielded an RMSE of 0.0352 and REP of –35.20%, confirming that measurement accuracy under these conditions remains low.

The second graph displays measurements of 0.195 m, 0.204 m, 0.211 m, 0.216 m, and 0.221 m. The resulting average was 0.2094 m, larger than the actual value but more consistent and closer to the ground truth compared to the first graph. Deviations detected along the Z-axis ranged from 0.065 m to 0.198 m, indicating a substantial reduction in non-motion noise relative to the first graph. The RMSE was 0.0094 with REP of –4.70%, reflecting improved measurement accuracy.

The third graph shows results of 0.316 m, 0.319 m, 0.338 m, 0.348 m, and 0.351 m. The average of 0.3344 m confirms a considerable positive deviation from the actual displacement. Z-axis deviations ranged from 0.262 m to 0.375 m, suggesting the presence of noise, albeit more controlled than in the first graph. Quantitative evaluation produced an RMSE of 0.0344 and REP of –11.47%, indicating that although stability was relatively good, the deviation level remained high.

The fourth graph presents highly consistent results, with identical measurements of 0.409 m across all tests. Accordingly, the average was also 0.409 m, highlighting a systematic and substantial positive deviation. Z-axis deviations were observed between 0.109 m and 0.461 m, reflecting variation in non-motion noise. Quantitative analysis indicated a low RMSE of 0.009 and REP of –2.25%, showing that despite the large absolute deviation, measurement consistency was relatively high.

https://doi.org/10.35877/jetech4580

ISSN : 2776-7914 (Print) / 2807-3045 (Online)

The fifth graph shows measurements of 0.490 m, 0.497 m, 0.501 m, 0.510 m, and 0.512 m. The average value of 0.502 m demonstrates a very large positive deviation from the actual displacement of 0.10 m. Z-axis deviations ranged from 0.328 m to 0.775 m, suggesting substantial noise interference in the non-motion direction. Interestingly, quantitative evaluation yielded a very small RMSE of 0.002 and REP of –0.40%, indicating that although the measurements diverged greatly from the ground truth, the relative stability between trials was excellent.

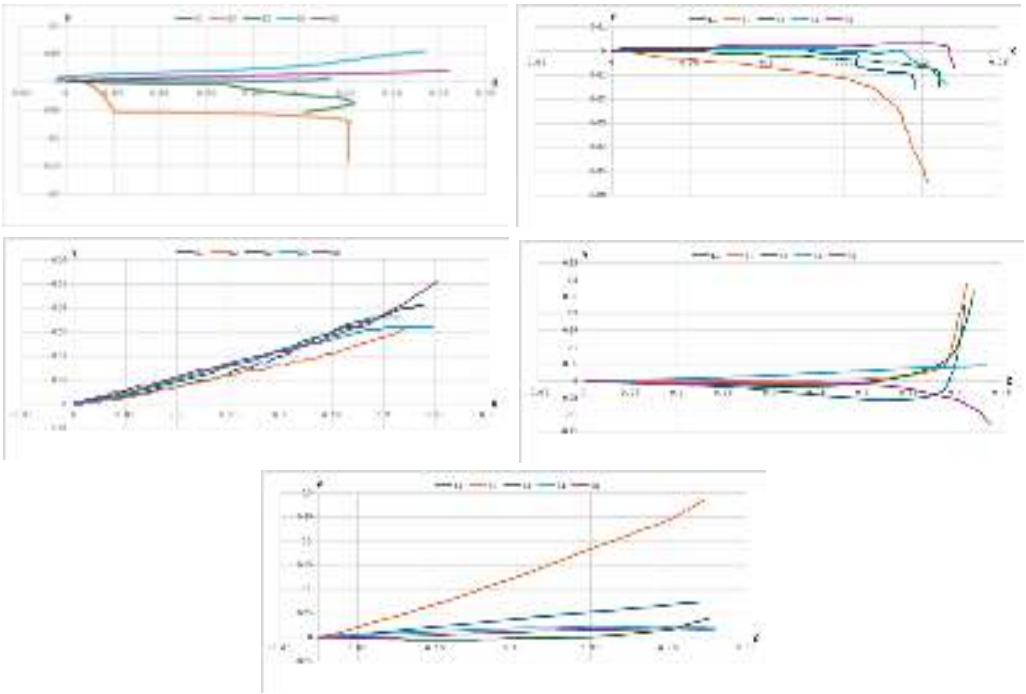

Fig. 3. Visualization of distance tracking with the ZUPT method integrated with the Low-Pass Butterworth Filter.

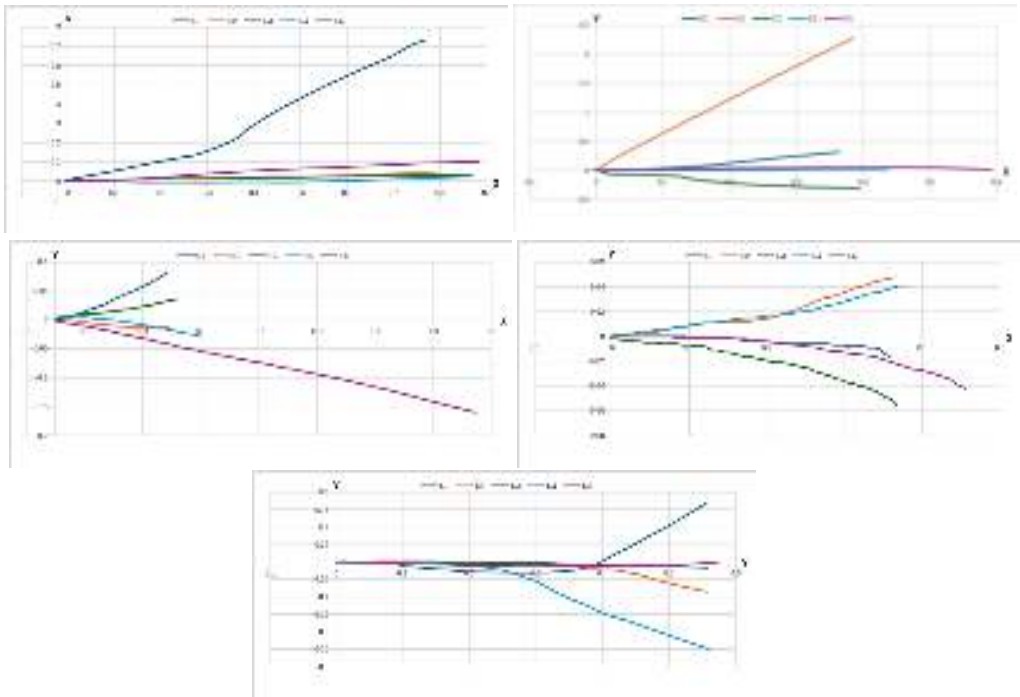

Fig. 4. Visualization of distance tracking without the ZUPT method integrated with the Low-Pass Butterworth Filter.

https://doi.org/10.35877/jetech4580

ISSN : 2776-7914 (Print) / 2807-3045 (Online)

Figure 4 presents five graphs of displacement testing over a distance of 10 cm along the X-axis, each conducted five times, with additional evaluation of deviations along the Z-axis and quantitative assessment using RMSE and REP.

The first graph (topmost) shows measurement results of 0.365 m, 0.386 m, 0.395 m, 0.437 m, and 0.593 m. The average value obtained was 0.4352 m, indicating a considerable positive deviation from the actual displacement of 0.10 m. Deviations along the Z-axis ranged from 0.212 m to 3.967 m, suggesting highly significant noise in the non-motion direction. Quantitative evaluation produced an RMSE of 0.3352 and REP of –335.20%, indicating a very high error level.

The second graph presents measurement results of 0.385 m, 0.392 m, 0.421 m, 0.503 m, and 1.445 m, with an average of 0.6292 m. This value demonstrates a very large positive deviation from the actual displacement. Deviations along the Z-axis ranged between 0.527 m and 1.237 m, reflecting substantial disturbances in the non-motion direction. Quantitative analysis yielded an RMSE of 0.4292 and REP of –214.60%, indicating a larger error compared to the first graph.

The third graph shows results of 0.359 m, 0.365 m, 0.367 m, 0.382 m, and 0.456 m. The average value obtained was 0.3858 m, still demonstrating a considerable positive deviation from the actual displacement. Deviations along the Z-axis ranged from 0.249 m to 0.430 m, suggesting that noise was relatively more controlled compared to the first and second graphs. Quantitative evaluation yielded an RMSE of 0.0858 and REP of –28.60%, indicating improved accuracy despite the presence of notable deviations.

The fourth graph presents highly consistent results of 0.556 m across all tests, resulting in an identical average of 0.556 m. This indicates a systematic and substantial positive deviation. Z-axis deviations were recorded between 0.211 m and 0.537 m, reflecting disturbances in the non-motion direction. Quantitative assessment produced an RMSE of 0.156 with REP of –39.00%, which, although better than the first and second graphs, still reflects a relatively high error level.

The fifth graph shows measurements of 0.768 m, 0.793 m, 0.869 m, 0.872 m, and 0.882 m. The average value of 0.8368 m indicates a very large positive deviation from the actual displacement. Deviations along the Z-axis ranged from 0.163 m to 0.429 m, suggesting the presence of noise, though within a relatively smaller range compared to the first and second graphs. Quantitative analysis produced an RMSE of 0.3368 and REP of –67.36%, showing that although the measurements were relatively consistent across trials, the absolute deviation from the actual value remained very high.

(1). Does not rely on satellite signals → suitable for use in caves or tunnels.
(2). High portability → small, lightweight, and easy-to-install sensors.
(3). Relatively low cost compared to geodetic GNSS or conventional geotechnical sensors.
(4). Supports real-time monitoring with IoT integration.

4.6. *Challenges and Limitations*

Although the results are quite promising, there are several limitations:

(1). Integration drift → Although ZUPT (Zero-Velocity Update) is effective, errors remain, especially for very small displacements (<10 cm).
(2). Sensitivity to noise → Accelerometers are susceptible to vibrations or electromagnetic interference.
(3). Long-term estimation → In multi-day monitoring, errors can accumulate, requiring additional correction algorithms (e.g., Kalman Filter or Complementary Filter).

4.7. *Implications of Research Results*

The results of this study indicate that the application of filters to the IMU significantly improves the accuracy of displacement estimation by suppressing errors caused by noise and

https://doi.org/10.35877/jetech4580

ISSN : 2776-7914 (Print) / 2807-3045 (Online)

sensor drift. The implication of this finding is that IMU-based systems have the potential to be used as a displacement measurement solution in applications requiring portable and low-cost devices, such as structural monitoring, medical rehabilitation, and simple navigation systems. However, without the application of appropriate filters, IMU data is less reliable due to the significant estimation deviation. Therefore, the use of filters is not only optional, but also an essential component in the design of IMU-based measurement systems.

5. Conclusion

This study demonstrated that the application of a second-order low-pass Butterworth filter significantly improves the accuracy of displacement estimation using an IMU sensor. Without filtering, the displacement results deviated substantially from the ground truth, with RMSE values reaching up to 0.4292 m and REP exceeding –300%, consistent with findings from previous studies reporting that IMU-based double integration tends to suffer from severe drift and noise accumulation. In contrast, after filtering, the results showed much higher accuracy, with RMSE values reduced to as low as 0.002 m and REP close to –0.40%, confirming that proper noise suppression is essential in IMU-based displacement estimation. Compared to earlier research that relied solely on ZUPT methods, the integration of a Butterworth filter in this study provided more stable and accurate displacement values, particularly for small to medium displacements (10–30 cm). These findings highlight that the combination of filtering and ZUPT not only mitigates drift error but also ensures consistent measurement results, thus extending the applicability of IMU sensors for displacement monitoring in environments where GNSS and InSAR are ineffective, such as caves and tunnels. Overall, this study reinforces the potential of IMU as a low-cost, portable, and flexible solution for ground displacement monitoring, while also confirming that filtering is not optional but a necessary component to achieve reliable results. Future research should focus on integrating advanced filtering techniques such as the Kalman Filter or machine learning-based approaches to further minimize long-term drift, thereby expanding IMU applicability to real-time landslide monitoring and other geotechnical applications.

References

Ahmad Sheikh, R., Abdullah Al-Hadi, A., Sabapathy, T., Simorangkir, R. B. V. B., Khan, R., Akkaraekthalin, P., Muhammad Nor Che Isa, C., Padmanathan, S., Md Hossain, T., & Jack Soh, P. (2025). A Triband Wearable Antenna for Location Tracking Using Cospas-Sarsat and GNSS. IEEE Open Journal of Antennas and Propagation, 6(3), 879–893. https://doi.org/10.1109/OJAP.2025.3553440

Bao, F., Nie, Z. Y., Hu, X., Huang, W. J., Peng, Y., Wang, Y., & Li, H. R. (2025). Extensometer comparison among provinces laboratories in China. Measurement: Sensors, 38, 101665. https://doi.org/10.1016/j.measen.2024.101665

Cahyadi, M. N., Asfihani, T., Suhandri, H. F., & Erfianti, R. (2024). Unscented Kalman filter for a low-cost GNSS/IMU-based mobile mapping application under demanding conditions. Geodesy and Geodynamics, 15(2), 166–176. https://doi.org/10.1016/j.geog.2023.05.001

Elhag, M., Chaabani, A., & Zhang, L. (2025). Assessment of surface deformation patterns using InSAR data: Implications for human impacts in Makkah City, Saudi Arabia. Kuwait Journal of Science, 52(3), 100419. https://doi.org/10.1016/j.kjs.2025.100419

Goanta, V. (2020). Extensometer for Determining Strains on a Tensile and Torsion Simultaneous Load. Sensors, 20(2), 385. https://doi.org/10.3390/s20020385

Haji-Aghajany, S., Izanlou, S., Tasan, M., Rohm, W., & Kryza, M. (2025). High-resolution GNSS troposphere tomography through explainable deep learning-based downscaling framework. Satellite Navigation, 6(1), 22. https://doi.org/10.1186/s43020-025-00177-6

MacAfee, E., Lohr, A. J., & De Jong, E. (2024). Leveraging local knowledge for landslide disaster risk reduction in an urban informal settlement in Manado, Indonesia. International Journal of Disaster Risk Reduction, 111, 104710. https://doi.org/10.1016/j.ijdrr.2024.104710

Parlin, A. F., Horning, N. A., Alstad, J. P., Cosentino, B. J., & Gibbs, J. P. (2024). Low-Cost, Lora Gnss Tracker for Wildlife Monitoring. SSRN. https://doi.org/10.2139/ssrn.5050356

https://doi.org/10.35877/jetech4580

ISSN : 2776-7914 (Print) / 2807-3045 (Online)

Piter, A., Haghshenas Haghighi, M., & Motagh, M. (2024). Challenges and Opportunities of Sentinel-1 InSAR for Transport Infrastructure Monitoring. PFG – Journal of Photogrammetry, Remote Sensing and Geoinformation Science, 92(5), 609–627. https://doi.org/10.1007/s41064-024-00314-x

Ruzza, G., Guerriero, L., Revellino, P., & Guadagno, F. M. (2020). A Multi-Module Fixed Inclinometer for Continuous Monitoring of Landslides: Design, Development, and Laboratory Testing. Sensors, 20(11), 3318. https://doi.org/10.3390/s20113318

Sari, P. T. K., Mochtar, I. B., & Lastiasih, Y. (2024). Special Case on Landslide in Balikpapan, Indonesia Viewed from Crack Soil Approach. KSCE Journal of Civil Engineering, 28(6), 2173–2188. https://doi.org/10.1007/s12205-024-0402-3

Sheikh, M. R., Nakata, Y., Shitano, M., & Kaneko, M. (2021). Rainfall-induced unstable slope monitoring and early warning through tilt sensors. Soils and Foundations, 61(4), 1033–1053. https://doi.org/10.1016/j.sandf.2021.05.010

Tjahjono, B., Firdiana, I., & Trisasongko, B. H. (2024). Modeling Landslide Hazard Using Machine Learning: A Case Study of Bogor, Indonesia. Jurnal Pengelolaan Sumberdaya Alam Dan Lingkungan (Journal of Natural Resources and Environmental Management), 14(2), 407. https://doi.org/10.29244/jpsl.14.2.407

Van Natijne, A. L., Bogaard, T. A., Van Leijen, F. J., Hanssen, R. F., & Lindenbergh, R. C. (2022). World-wide InSAR sensitivity index for landslide deformation tracking. International Journal of Applied Earth Observation and Geoinformation, 111, 102829. https://doi.org/10.1016/j.jag.2022.102829

Yang, F., Guan, D., Li, X., & Dou, C. (2025). Application Research on High-Precision Tiltmeter with Rapid Deployment Capability. Sensors, 25(5), 1559. https://doi.org/10.3390/s25051559

Yang, Z., Ding, X., Yang, Y., & Wang, Q. (2025). OiSAM-FGO: An efficient factor graph optimization algorithm for GNSS/INS integrated navigation system. Satellite Navigation, 6(1), 23. https://doi.org/10.1186/s43020-025-00173-w

Yong, C. Z., Harima, K., Rubinov, E., McClusky, S., & Odolinski, R. (2022). Instantaneous Best Integer Equivariant Position Estimation Using Google Pixel 4 Smartphones for Single- and Dual-Frequency, Multi-GNSS Short-Baseline RTK. Sensors, 22(10), 3772. https://doi.org/10.3390/s22103772

Zhang, X., Yang, Y., Yang, H., Ren, X., Lin, X., Le, X., & Li, X. (2025). Performance of PPP and PPP-RTK with new-generation GNSS constellations and signals. Satellite Navigation, 6(1), 17. https://doi.org/10.1186/s43020-025-00169-6

Zhang, Z., Wang, X., Wu, Y., Zhao, Z., & E, Y. (2021). Applied Research on InSAR and GPS Data Fusion in Deformation Monitoring. Scientific Programming, 2021, 1–9. https://doi.org/10.1155/2021/3888975